WIND TUNNEL TESTING TO DETERMINE UNSTEADY LOADS ON A HELICOPTER FUSELAGE IN A SHIP AIRWAKE

Richard G. Lee* , Steven J. Zan†
Aerodynamics Laboratory, Institute for Aerospace Research
National Research Council of Canada
Ottawa, Canada

Keywords: *dynamic interface, ship airwake, helicopter, unsteady aerodynamic loads*

Abstract

Pilots of maritime helicopters face significant challenges when operating from a small non-aviation ship. In addition to the effort required for tracking and landing on a small moving flight deck, at times in a rough sea, a maritime helicopter pilot must also cope with unsteady aerodynamic loads arising from the turbulent airwake of the ship. This paper describes subscale wind tunnel experiments designed to determine the unsteady aerodynamic loads acting upon a rotorless helicopter fuselage in a ship airwake. An unsteady aerodynamic load coefficient is defined and computed from spectral curve fits of collapsed normalized power-spectral densities. The power-spectral densities are developed from measurements. Unsteady load coefficients for side force, yawing moment, and drag force are examined as a function of wind speed and direction, and fuselage position. The ramifications of collapsed normalized power-spectral densities are also discussed.

1 Nomenclature

A_f	fuselage reference area (0.024 m^2)
$\widetilde{C}_D$	unsteady drag force coefficient
$\widetilde{C}_n$	unsteady yawing moment coefficient
$\widetilde{C}_Y$	unsteady side force coefficient
f	frequency
f^*	reduced frequency, fL/V
L	length
L_f	overall fuselage length (0.331 m)
q	dynamic pressure, $\frac{1}{2}\rho V^2$
$S(f)$	power-spectral density
V	relative wind speed
z	height above wind tunnel floor
α	power law exponent
ρ	density
ψ	wind direction

2 Introduction

Owing to the complex air flow around a ship superstructure, the operation of helicopters onto and from ships is a significant challenge for a pilot. The pilot must navigate the helicopter through this flow field, known as the airwake. The airwake contains spatial gradients in flow speed and direction, as well as significant unsteadiness over the bandwidth of concern with respect to handling qualities, 0.2 to 2 Hz [1]. An airwake is comprised of free shear layers, recirculation zones, large wakes, and vortex structures all of which contribute to the operational challenges for the pilot. Because the fuselage and rotor sizes are comparable in size to the scales of turbulence in the flow, and because these scales are rapidly changing in the near-wake region, the fuselage loading cannot be represented accurately by assuming the flow field conditions at one point (the centre of gravity, for example) can be applied to the entire fuselage or rotor. In other words the fuselage loading and rotor output arise from imperfect correlations.

Focusing on the example of a frigate, with a landing deck directly behind the hangar, several flow topologies have been shown to exist over the flight deck for various wind directions [2]. For wind directions on or close to the bow, the flow can be considered similar to that for a backward-facing step

*Assistant Research Officer
†Senior Research Officer

(Fig. 1(a)). In this case, the helicopter traverses free shear layers which separate from the top and sides of the hangar. Under the shear layers, and close to the rear face of the hangar is a recirculation region, which also engulfs part of the fuselage.

As the wind direction increases above about 15 deg, the flow field topology changes and vortices begin to emerge from the flight deck edges, and aft corners of the hangar (Fig. 1(b)). Because of the separated flow over the flight deck, the vortex structures vary in space and time, which again will contribute to unsteady loading on the helicopter, though the frequency content and scales of the flow structures may be significantly different from those of free shear layers and bluff-body wakes.

This paper discusses unsteady airwake loading on a helicopter fuselage in close proximity to a frigate as derived from sub-scale wind tunnel experiments. The work was spawned as part of a larger research program investigating the aerodynamic aspects of the helicopter-ship dynamic interface. In particular it was of interest to examine the unsteady aerodynamic load coefficients as a function of wind speed and direction, and fuselage position. These load coefficients can be used as input to a dynamic interface flight simulator, but they also cast some light on the nature of the unsteady loading experienced by maritime helicopter pilots. Previous components of the work have dealt with loading on the rotor [3, 4].

3 Experimental Setup

3.1 Wind Tunnel Facility

The experiment was performed in the open-circuit Propulsion Wind Tunnel at the Institute for Aerospace Research. The test section of this facility (Fig. 2) measures 3.1 m wide by 6.1 m high with an overall length of 12.2 m. Speeds as high as 42 m/s can be achieved in the test section.

Spires, such as those shown in Fig. 2, are commonly used in wind engineering to simulate an atmospheric boundary layer [5]. For this experiment two spires were installed at the entrance of the test section to produce a turbulent atmospheric boundary layer consistent with a moderately rough sea. The flight deck of the ship model was located approximately four spire-heights downstream of the spires. At this location, with the ship and helicopter removed from the test section, a boundary layer survey was performed with a hot-film anemometer to confirm that the wind speed profile corresponds to the power law model:

$$\frac{V}{V_{ref}} = \left(\frac{z}{z_{ref}}\right)^{\alpha} \tag{1}$$

where z_{ref} is the height of the relative wind speed anemometer on the ship's mast. The survey revealed $\alpha = 0.09$ (0.10 is suggested for coastal areas [6]). A longitudinal turbulence intensity of 11% at z_{ref} was in reasonable agreement with predictions [6] for atmospheric turbulence over water. From the hot-film measurements the longitudinal length scale was estimated to be 16 m at full scale.

3.2 Scaling Parameters

Frequency scaling is necessary to capture correctly the unsteady aerodynamic loading over the desired full-scale bandwidth of 0.2 to 2 Hz. It is also the most important scaling parameter because the spectra of the unsteady loads arising from the turbulent airwake are the focus of the investigation. Reduced frequency matching relates the frequency, geometric, and velocity scales as follows:

$$\frac{f^*_{fs}}{f^*_{ms}} = \left(\frac{f_{fs}}{f_{ms}}\right)\left(\frac{L_{fs}}{L_{ms}}\right)\left(\frac{V_{ms}}{V_{fs}}\right) = 1 \tag{2}$$

where subscripts fs and ms refer to full-scale and model-scale respectively. A geometric scale of $L_{ms}/L_{fs} = 1/50$ was fixed by an existing ship model, and a velocity scale of $V_{ms}/V_{fs} = 5/4$ was governed by the maximum velocity atttainable in the test section. Subsequently Eqn. 2 yields the frequency scale, $f_{ms}/f_{fs} = 62.5$.

The highest fuselage Reynolds number, based on overall length, was approximately 1.0×10^6. One must be cautious, however, in defining a specific Reynolds number in the case of a fuselage immersed in an airwake. There are significant velocity gradients and even flow recirculation over the volume occupied by the fuselage. Thus the interpretation of Reynolds number is not as straightforward as in the case with uniform flow.

Since the fuselage length is comparable to the ship beam, the beam-based ship Reynolds number exceeds $11,000$, the minimum recommended for the wind-tunnel modeling of ships [7].

3.3 Ship and Helicopter Models

The ship model, depicted schematically in Fig. 3, is a 1/50-scale above-water model of the Canadian Pa-

trol Frigate (CPF) used in previous airwake experiments [8]. Small structures located in front of the helicopter hangar, such as wire antennas, handrails, a small lattice radar-mast, and 57 mm cannon, were not included in the model. From an aerodynamic perspective, the airwake should nevertheless be highly representative of a detailed CPF since the wake signatures of the small structures will blend into the flow field as one moves aft. As a further simplification to the ship model, exhaust flows from the funnel and mechanical units were not included, however, it is recognized that funnel exhaust could have an impact on the unsteady aerodynamic loading of the fuselage. Ship motion was not considered in this test, and the pitch and roll angles of the ship model were zero.

The 1/50-scaled model of the Sea King helicopter (Fig. 4) was rotorless and featured representations of the major fuselage components. Details such as the air/surface search radar, electric cable winch, sonobuoy launchers, and various antennas were considered nonessential for unsteady load measurements and subsequently omitted from the model. The fuselage was manufactured from structural plastic foam under numerical control. During testing the pitch and roll angles of the fuselage were zero. Also, the longitudinal axis of the helicopter model was always aligned with that of the CPF model, which is typical for a landing manoeuvre.

3.4 Dynamic Balance and Model Support

A 'dynamic' balance is necessary to acquire the aerodynamic loading spectra of a helicopter fuselage in the ship airwake. This type of balance has high stiffness and is used in combination with a lightweight model. Ideally the lowest natural frequency of the assembly will be sufficiently above the frequency bandwidth of interest to prevent balance resonance from affecting measurements. If the resonant frequency is not sufficiently high, post-test spectral corrections are required. Fitting conveniently within a metal-lined cavity inside the fuselage model, the internal balance measures side force, yawing moment, and drag force in the body-axis coordinates. Yawing moment was resolved about the axis of the rotor shaft. The balance sits on top of a sting (Fig. 5(a)), which in turn threads into a large steel block placed beneath the flight deck of the CPF model. The steel block serves as a firm mechanical ground. Of the ways the model can be mounted on a sting, the adopted approach is considered to have the least aerodynamic interference with the fuselage wake. The aerodynamic loads were not corrected for sting interference.

The balance was statically calibrated to a limit load of ± 20 N for side and drag force, and ± 1 Nm for yawing moment. The accuracy of the balance was estimated to be within $\pm 0.5\%$ of the calibration limits. A dynamic calibration was performed to identify the resonant frequencies of the model/balance/sting assemblage, and to determine the degree to which mechanical resonance will infringe on the bandwidth of interest (12.5 to 125 Hz at model scale). Since the lowest resonant frequency of the assemblage was about 137 Hz, post-test spectral corrections were necessary to account for the effects of the mechanical transfer function.

3.5 Data Acquisition and Reduction

The balance output signals were sampled at a rate of 1 kHz for a duration of 34 seconds. This corresponds to a sample rate of 16 Hz and a duration of 35.4 minutes at full scale. The voltage signals were converted to time-varying drag force, side force, and yawing moment, in engineering units at model scale; then power-spectral densities (PSD) were computed from the average of sixteen 2048-point fast-Fourier transforms of the unbiased time-histories of the aerodynamic loads. The correction for the effect of the structural resonance was accomplished by fitting the one degree-of-freedom mechanical admittance function to a resonant peak in a least-squares fashion [9]. After correction, the PSDs were converted to spectral coefficients by:

$$S_{C_{Y,D}}(f) = \frac{S_{Y,D}(f)}{(qA_f)^2}, \quad S_{C_n}(f) = \frac{S_N(f)}{(qA_f L_f)^2} \qquad (3)$$

where A_f and L_f are the fuselage model reference area and length respectively.

Unsteady aerodynamic load coefficients were calculated from the power-spectral densities. They are defined as the square-root of the integral of the PSD taken over a specific frequency bandwidth (f_1, f_2):

$$\widetilde{C}_{Y,n,D} = \left[\int_{f_1}^{f_2} S_{C_{Y,n,D}}(f)\, \mathrm{d}f \right]^{\frac{1}{2}} \qquad (4)$$

where $\widetilde{C}_{Y,n,D}$ represents collectively the unsteady side force, yawing moment, and drag force coefficients. The bandwidth $(f_1, f_2) = (12.5, 125)$ as indicated earlier. These unsteady loading coefficients are statistical quantities that indicate the degree of variation in the

aerodynamic loading within the frequency bandwidth of interest. A high unsteady loading coefficient signifies a large degree of unsteadiness in a given aerodynamic load, whereas an unsteady coefficient with a magnitude of zero indicates the aerodynamic loading is invariant in time.

3.6 Test Program

The test points for these experiments cover a range of wind directions and at least two wind speeds for each direction. At some wind directions, a third low-speed case was chosen for the purpose of evaluating the variation of unsteady loading with wind speed. All test points were covered at three on-deck hover positions; additional measurements were taken at three wind directions in an off-deck position. These four hover positions represent a typical landing manoeuvre which begins with the fuselage model in high hover off the port edge of the flight deck, moving laterally to the port edge, then to the centre of the deck at high hover; and finally to low hover centred over the deck before touchdown.

4 Results and Discussion

The scope of the results appearing in this paper are limited to $-25 \leq \psi \leq 30$ deg with the fuselage model centred over the flight deck in the high and low hover positions (Fig. 5). The convention for wind direction is as follows: $\psi < 0$ deg signifies a wind from the port side of the ship, and $\psi > 0$ deg is a wind from the starboard side. The reference wind speed (referred to here as wind speed) is the ship anemometer speed [8]. Unless stated otherwise, dimensional quantities such as V and f are at model scale.

4.1 Typical Loading Spectra

Figure 6 presents examples of power-spectral densities for coefficients of side force, yawing moment, and drag force over the frequency bandwidth of 12.5 to 125 Hz. Recall that the unsteady load coefficients $\widetilde{C}_Y$, $\widetilde{C}_n$, and $\widetilde{C}_D$ are computed according to Eqn. 4. A discussion of the character of the PSDs can be found in [10].

4.2 Spectra Normalization

Figure 7(a) depicts the PSDs of drag coefficient for two wind speeds and constant wind direction and position. The spectra are normalized by converting frequency to reduced frequency, $f^* = fL_f/V$, and multiplying $S_{C_{Y,n,D}}(f)$ by the factor V/L_f. After normalizing the spectra in this manner, a collapse of the results occurs, as shown in Fig. 7(b), for the wind direction and position tested. Moreover, the integral of each normalized spectrum preserves the square of the unsteady load coefficient. Having achieved a collapse of the spectra, the results can now be used collectively to find a suitable curve fit. The most common spectral curve fit used has the non-linear form:

$$S_{C_{Y,n,D}}(f^*) = \frac{a f^{*n_1}}{(1+b f^{*m})^{n_2}} \qquad (5)$$

where the exponent $m = 3.5$ or 4.0 depending on the wind direction. Equation 5 was fitted to a set of normalized spectral data in a least-squares manner with constants (a,b) and exponents (n_1,n_2) as floating parameters (Fig. 7(c)). Spectral curve fits for $0 \leq \psi \leq 30$ deg at low hover are shown in Fig. 7(d).

The collapse of normalized PSDs has two significant ramifications. First, it suggests a simplication to the methodology of acquiring unsteady fuselage loads in a wind tunnel. Specifically, unsteady loading can be acquired at two wind speeds: The highest sustainable wind speed provides high-output signal levels from the balance, and a lower speed improves the accuracy of the dimensionless representation at high f^*. The selection of the lower wind speed should be contingent upon an acceptable balance output signal-to-noise ratio.

Secondly, the dimensionless spectral representations can be re-scaled and input to a flight simulator in order to provide the pilot with the correct representation of the unsteady drag force, side force and yawing moments. These fuselage loads are currently determined by a point-loading concept; that is, basing them on the velocity at the aircraft centre of gravity and static force coefficients obtained from elsewhere, with the assumption that the loading and velocity are perfectly correlated over the entire fuselage [11]. While this approach is generally conservative, it may become unrealistically so for the case of a frigate airwake as the flow correlation lengths are often smaller than the fuselage width.

4.3 Effect of Wind Speed

The non-dimensional spectral densities suggest that the unsteady loading is insensitive to Reynolds number, at least over the range covered by this experiment. This is not surprising since low-speed separated flow wakes from sharp-edged bodies are insensitive to

Reynolds number [12]. The fuselage itself can also be considered a non-streamlined body for yawed winds. It would thus seem straightforward to integrate under the PSD to generate unsteady loads from which aerodynamic coefficients could be calculated in the standard way. However, in an operational context, the interest is to define the loading over a fixed dimensional frequency bandwidth of 0.2 to 2 Hz at full scale. In this case, the unsteady loading coefficient is based on the integration of the PSD over a sliding bandwidth as illustrated in Fig. 8. When integrated over such a bandwidth, the unsteady loads change with wind speed. As a general observation it can be seen that as wind speed increases, the bandwidth of interest moves to lower reduced frequencies, thereby increasing the unsteady loading coefficient. Since the actual loading is a product of the coefficient and dynamic pressure, then the unsteady loading increases in the form V^n where $n > 2$, whereas V^2 is normally representative of static aerodynamic loading.

4.4 Effect of Wind Direction

Figure 9 presents the variation of unsteady side, drag and yawing moment coefficients with wind speed (as determined from spectral curve fits) for a range of wind directions from 0 to 30 deg for the fuselage located at the high hover position. It is clear that as the wind direction departs from 0 deg, the coefficients increase. Using the 0-deg curve as a baseline, at high wind speeds the coefficients at 20 deg more than double, and are about 3 times larger at 30 deg. As expected the coefficients also increase with wind speed. The curves all tend to 'flatten' with increasing wind speed reflecting the nature of the unsteady load PSDs at low frequencies.

In the case of winds from the other direction (Fig. 10), the coefficients suggest symmetry, except for the unsteady drag coefficient which is distinctly reduced at -15 and -20 deg compared to +15 and +20 deg. The greater magnitude for positive wind directions is attributed to the asymmetry of the ship, specifically the Close-in Weapon System (CIWS) located on the aft starboard corner of the hangar roof (Fig. 3). The presence of the CIWS increases the level of turbulence in the flow impinging on the fuselage, producing a power-spectral density with more energy over a specific frequency range, leading to a 'flatter' variation in the unsteady drag coefficient with velocity for those wind directions. The changes in unsteady drag coefficient for ± 20 deg are more clearly shown in Fig. 11.

4.5 Effect of Position

The unsteady loading coefficients vary not only with wind speed and direction, but also with position, i.e., the location of the fuselage relative to the flight deck. For a wind direction of 0 deg in Table 1, relatively small changes occur in the coefficients between the high and low hover positions. As the fuselage is lowered toward the deck at a constant reference velocity, the wind speed acting on the fuselage will decrease; however the turbulence intensity rises and these two factors probably yield similar values of unsteady velocity which thus leads to similar unsteady loading coefficients.

As the wind direction increases to 30 deg, the unsteady load coefficients are distinctly less at low hover than at high hover. For a wind direction of 30 deg, the form of the unsteady side force and yawing moment coefficient curves change considerably between the two hover positions. Examination of the corresponding PSDs reveals that the character of the loading has also changed considerably, specifically the PSDs do not flatten at low frequencies. At about this wind direction, a vortex begins to form over the flight deck with an apex on the windward side of the deck near the aft corner of the hangar, as illustrated in Fig. 1(b) (see 'Region 3'). It is possible that for this wind direction at low hover the vortex is the dominant source of unsteady fuselage loading as opposed to the shear layers and wake emanating from the hangar. With further increases in wind direction the vortex tends to strengthen, which would further increase the unsteady loading coefficients.

ψ (deg)	Hover Position	$\widetilde{C}_Y$	$\widetilde{C}_n$	$\widetilde{C}_D$
0	high	0.0212	0.00340	0.0158
	low	0.0191	0.00370	0.0166
30	high	0.0585	0.01170	0.0479
	low	0.0486	0.00975	0.0407

Table 1: Coefficients of unsteady loading, as determined from spectral curve fits, for $\psi = 0$ and 30 deg with the fuselage model at high and low hover. *Wind speed: 40 kts at full scale. Deck position: centred over deck.*

5 Concluding Remarks

An experiment to measure the unsteady aerodynamic loads acting upon a rotorless helicopter fuselage in a ship airwake was described. Normalized power-spectral densities for side force, yawing moment, and drag force coefficients were developed from the measurements and found to collapse well, thereby allowing curve fits of the collapsed spectra to be generated. Bandwidth-limited unsteady aerodynamic load coefficients, a measure of variation of an aerodynamic load, were computed from these spectral fits. The coefficients were found to increase with wind speed indicating that the relevant unsteady loads are proportional to wind speed to a power greater than two. Variations of the unsteady load coefficients with wind direction and fuselage position were found. Given the complex structure of a ship airwake, this was expected.

The dimensionless representations of unsteady loading are based on experiments which account for imperfect correlations in the unsteady loading acting on the fuselage. Thus they will serve as more accurate models of unsteady aerodynamic loads than the 'point-load' models currently used in dynamic interface flight simulators.

6 Acknowledgements

This project is a collaboration of the Department of National Defence and the Institute for Aerospace Research.

References

[1] McRuer, D.T. Interdisciplinary interactions and dynamic systems integration. *International Journal of Control*, Vol. 59, No 1, pp 3–12, 1994.

[2] Healey, J. V. The aerodynamics of ship superstructures. In *AGARD-CP-509, Aircraft Ship Operations, Paper 4*. 1991.

[3] Zan, S.J. Experimental determination of rotor thrust in a ship airwake. *Journal of the American Helicopter Society*, April 2002.

[4] Syms, G. and Zan, S.J. Analysis of rotor forces in a ship airwake. In *AGARD-CP-552, Aerodynamics and Aeroacoutics of Rotorcraft, Paper 31*, 1994.

[5] Irwin, H.P.A.H. Design and use of spires for natural wind simulation. Laboratory Technical Report LTR-LA-233, National Research Council, National Aeronautical Establishment, April 1979.

[6] Simiu, E. and Scanlan, R.H. *Wind Effect on Structures*. Chapter 2. John Wiley & Sons Inc., 2nd edition, 1986.

[7] Healey, J.V. Establishing a database for flight in the wake of structures. *Journal of Aircraft*, Vol. 29, No 4, pp 559–564, July-August 1992.

[8] Zan, S.J., Syms, G.F., and Cheney, B.T. Analysis of patrol frigate air wakes. In *RTO-MP-15, Fluid Dynamics Problems of Vehicles Operating Near or in the Air-Sea Interface, Paper 7*, 1998.

[9] Larose, G.L., Agdrup, K., and Larsen, S.V. Direct measurements of the aerodynamic admittance of large ships. In Larsen, Larose, and Livesey, editors, *Wind Engineering into the 21st Century*, pages 1939–1944, 1999.

[10] Lee, R.G. and Zan, S.J. Unsteady aerodynamic loads on a helicopter fuselage in a ship airwake. In *Proceedings of the American Helicopter Society 58th Annual Forum, Montreal, Canada*, June 11-13, 2002.

[11] Bunnell, J.W. An integrated time-varying airwake in a UH-60 black hawk shipboard landing simulation. AIAA Paper 2001-4065.

[12] Schewe, G. Investigation of the aerodynamic forces on bluff bodies at high Reynolds number. European Space Agency, Technical Translation, ESA-TT-914, June 1985.

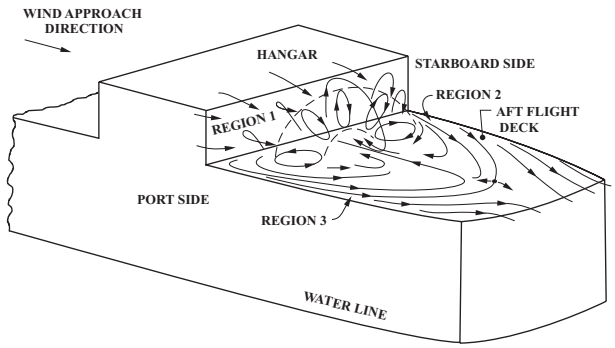

(a) Zero wind direction

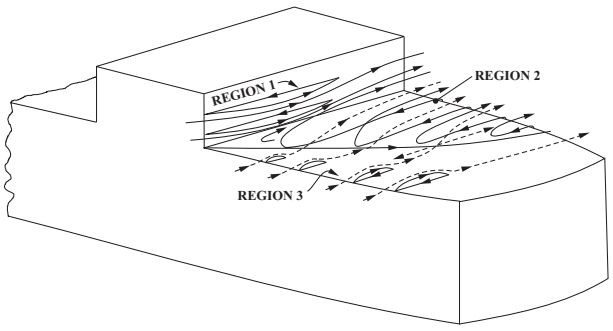

(b) Typical non-zero wind direction

Fig. 1 : General features of a ship airwake [2].

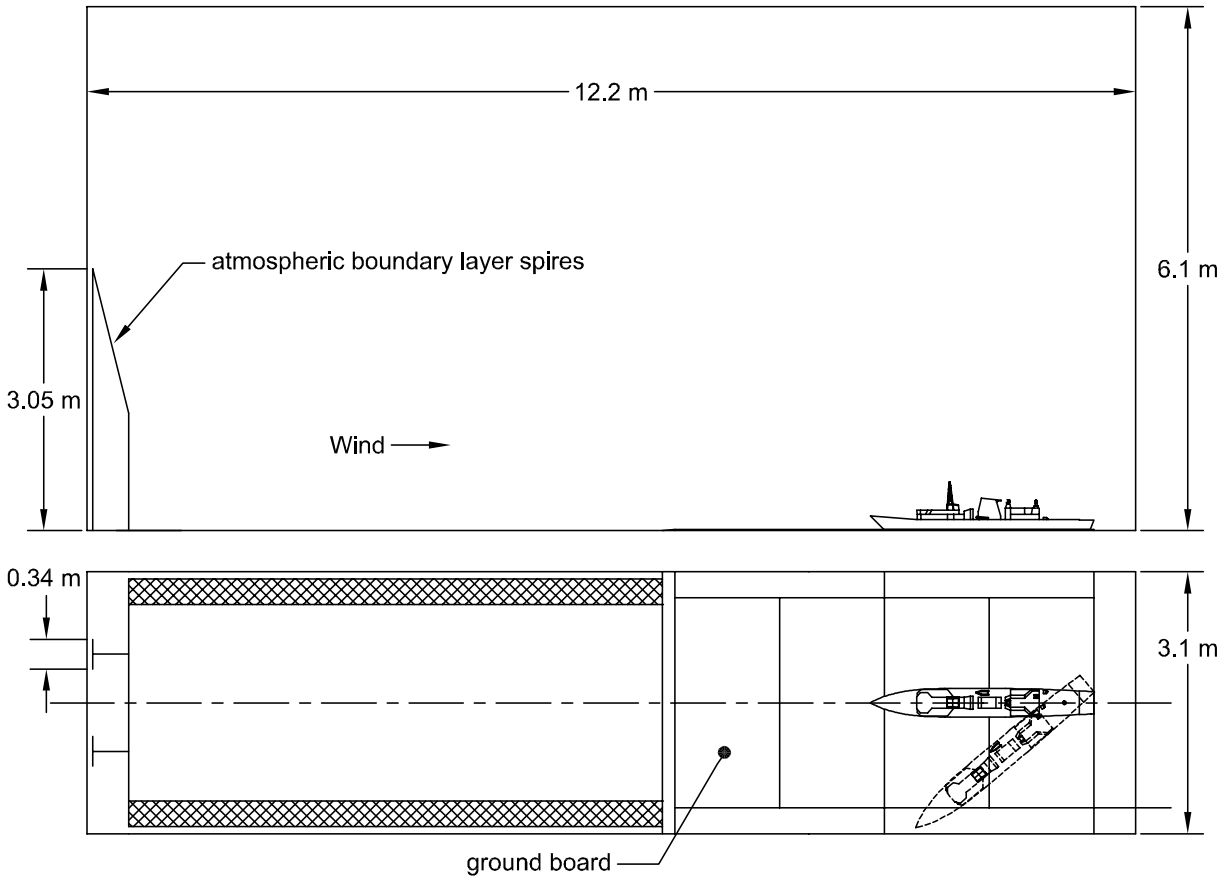

Fig. 2 : Layout of 3m×6m test section.

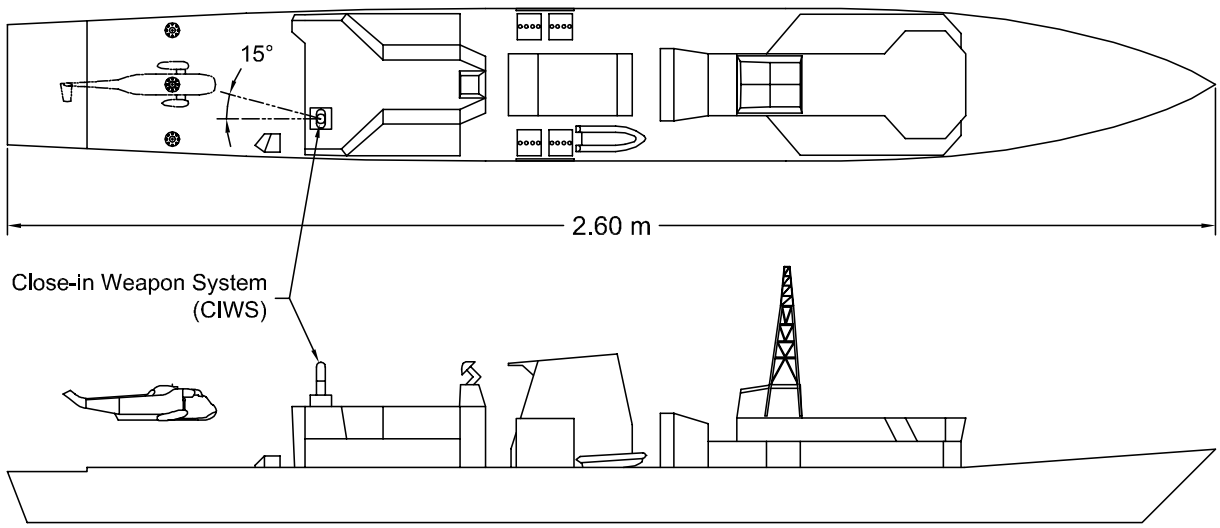

Fig. 3 : 1/50-scale above-water model of the Canadian Patrol Frigate with a Sea King fuselage shown in high hover, centred over the flight deck.

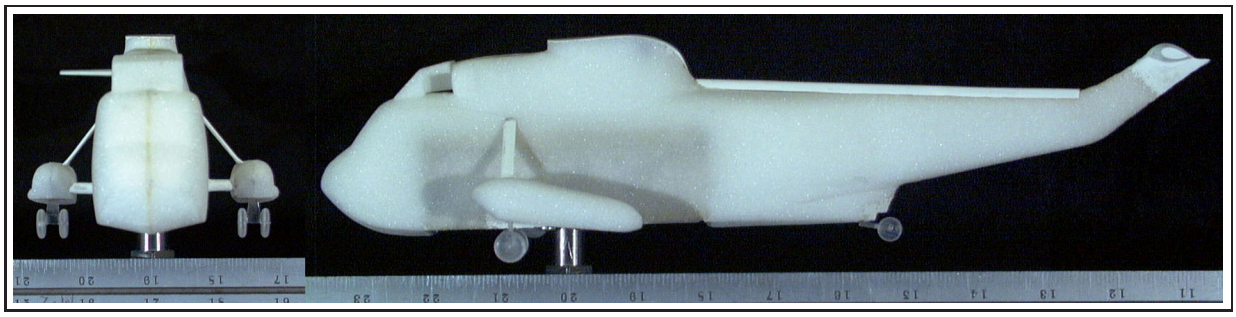

Fig. 4 : 1/50-scale model of the CH-124 Sea King fuselage. The reference area is the product of overall length and height of the fuselage model.

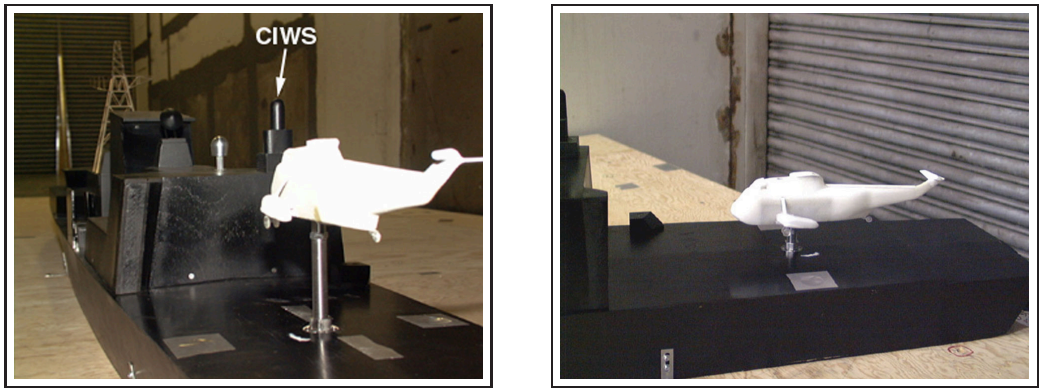

(a) Centred over flight deck, high hover

(b) Centred over flight deck, low hover

Fig. 5 : Hover positions tested. In low hover, the rotor plane is 6 m (full scale) above the flight deck; in high hover, the rotor plane is 9 m above the deck.

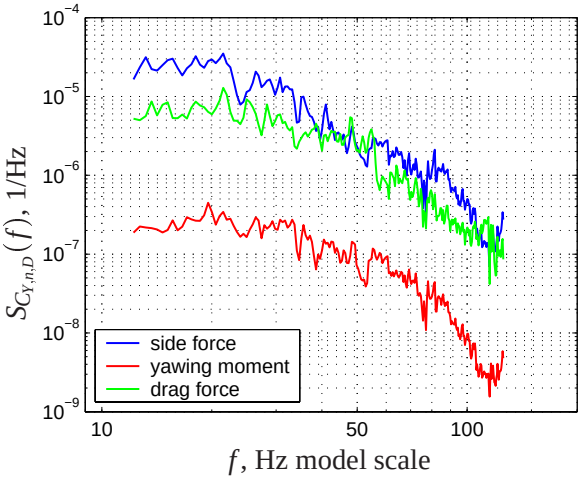

Fig. 6 : Typical PSDs for dimensionless side force ($\widetilde{C}_Y = 0.0238$), yawing moment ($\widetilde{C}_n = 0.00306$), and drag force ($\widetilde{C}_D = 0.0152$). *Wind Speed: 28 m/s. Wind direction: 0 deg. Position: centred over deck, high hover.*

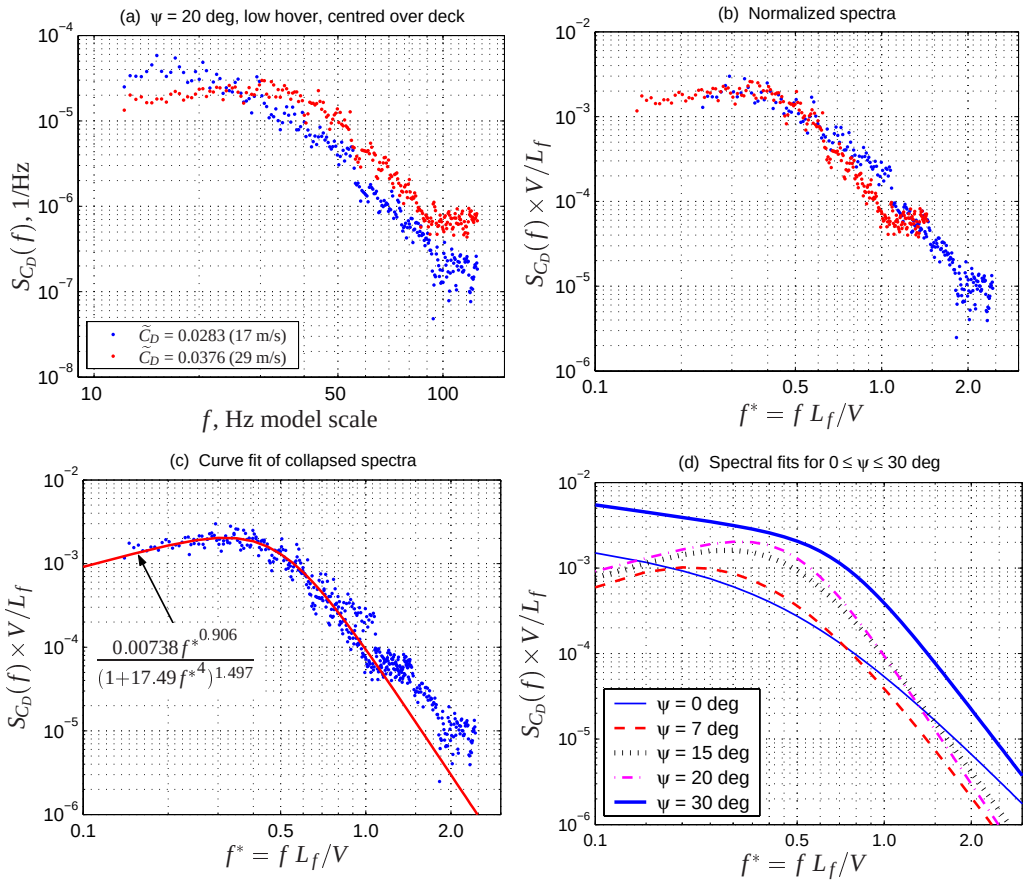

Fig. 7 : Spectra normalization and curve fit of collapsed spectra.

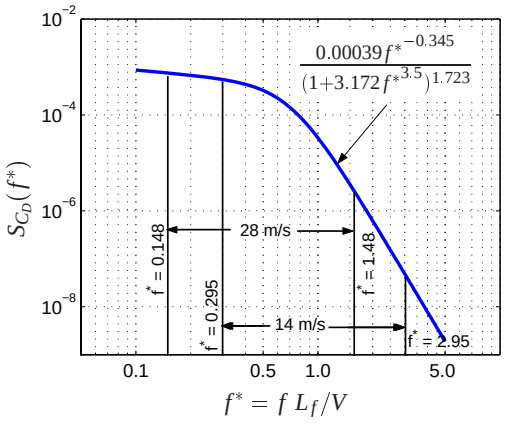

Fig. 8 : Computing the coefficient of unsteady drag force for two wind speeds with a spectral curve fit. For 28 m/s, $\widetilde{C}_D = 0.0161$ (compare with $\widetilde{C}_D = 0.0152$ in Fig. 6); $\widetilde{C}_D = 0.0129$ for 14 m/s. *Wind direction: 0 deg. Position: centred over deck, high hover.*

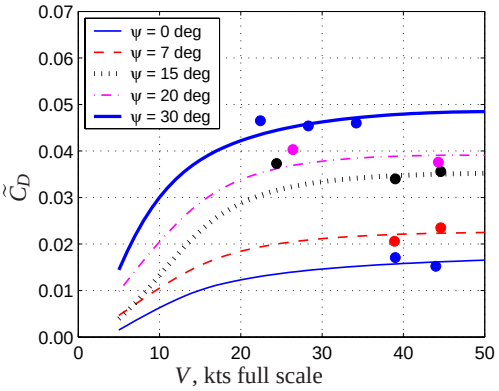

Fig. 9 : Variation of $\widetilde{C}_D$, $\widetilde{C}_Y$, and $\widetilde{C}_n$ with wind speed for $\psi \geq 0$ deg, as determined from spectral curve fits. Coloured dots represent experimental results. *Position: centred over deck, high hover.*

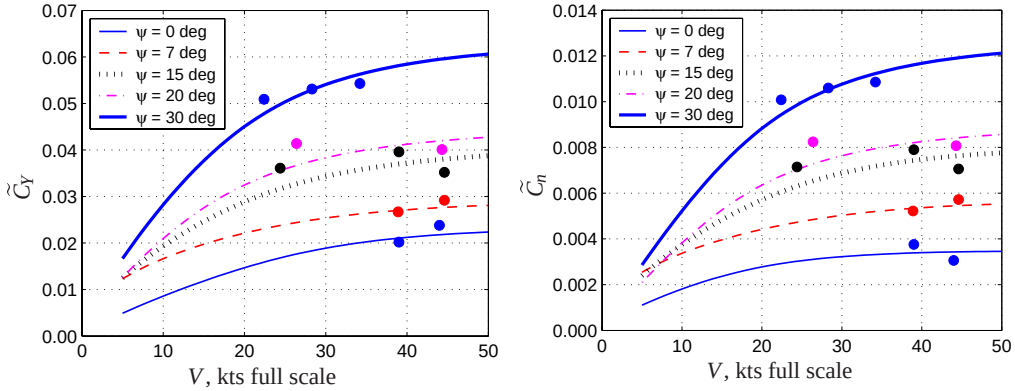

Fig. 9 : Continued.

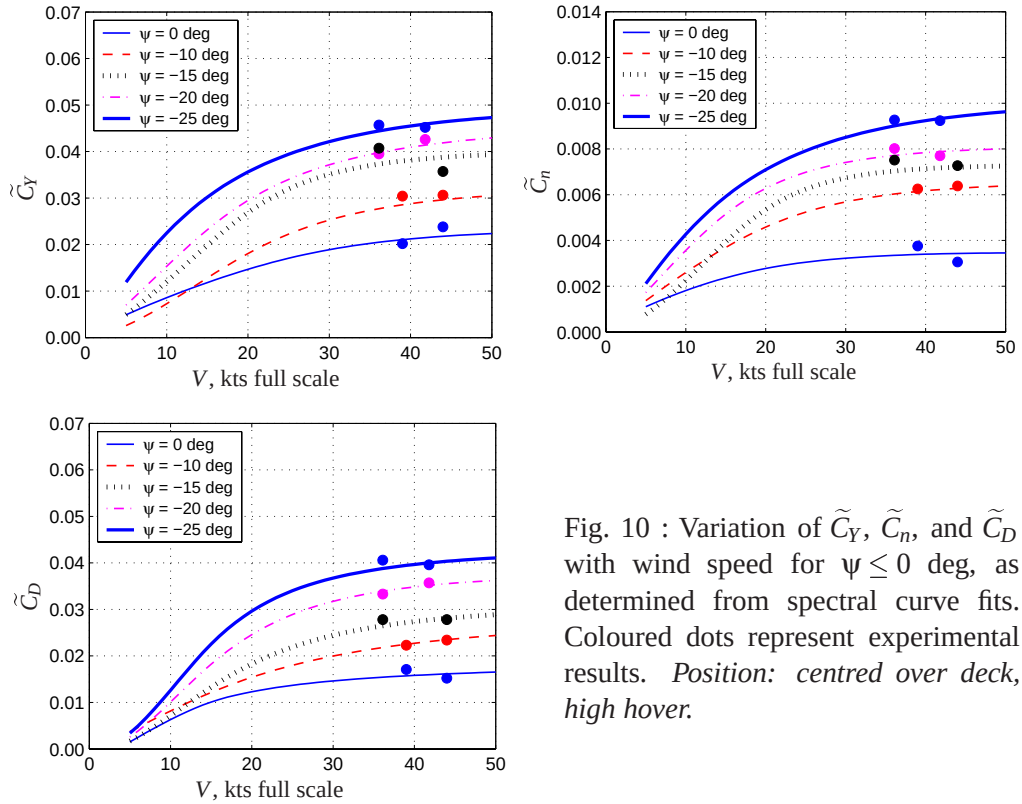

Fig. 10 : Variation of $\widetilde{C}_Y$, $\widetilde{C}_n$, and $\widetilde{C}_D$ with wind speed for $\psi \leq 0$ deg, as determined from spectral curve fits. Coloured dots represent experimental results. *Position: centred over deck, high hover.*

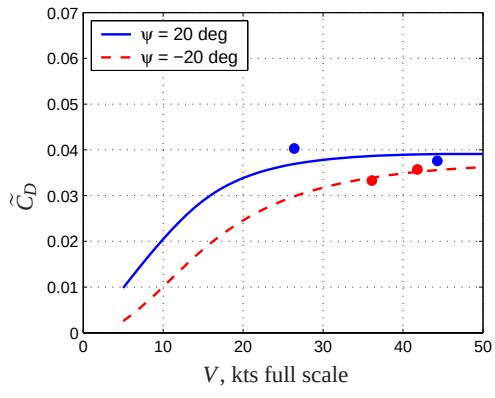

Fig. 11 : Comparison of unsteady drag force coefficient for $\psi = \pm 20$ deg, as determined from spectral curve fits. Coloured dots represent experimental results. *Position: centred over deck, high hover.*